

The evolution of baryon density fluctuations in multi-component cosmological simulations

Naoki Yoshida^{1,2*}, Naoshi Sugiyama², Lars Hernquist¹

¹*Harvard-Smithsonian Center for Astrophysics, 60 Garden Street, Cambridge MA 02138, USA*

²*National Astronomical Observatory Japan, Mitaka, Tokyo 181-8588, Japan*

Accepted for publication in MNRAS, May 20, 2003

ABSTRACT

We critically examine how the evolution of the matter density field in cosmological simulations is affected by details of setting up initial conditions. We show that it is non-trivial to realise an initial distribution of matter in N -body/hydrodynamic simulations so that the baryon and dark matter density fluctuations and their velocities evolve consistently as theoretically predicted. We perform a set of cosmological simulations and use them to distinguish and verify an appropriate method for generating initial conditions. We show that a straightforward way of applying the Zel’dovich approximation to each component using distinct transfer functions results in an incorrect growth of density fluctuations and that it is necessary to correct velocities at the initial epoch. The unperturbed uniform particle distribution must be also generated appropriately to avoid tight coupling of the baryonic and dark matter components. We recommend using independent “glass” particle distributions, using distinct transfer functions for baryons and dark matter, *and* taking into account the difference in the velocity fields at the initialisation epoch. The proposed method will be useful for studies of the evolution of the intergalactic medium and the formation of the first cosmological objects using numerical simulations.

Key words: cosmology:theory – early universe – intergalactic medium – methods: n-body simulations

1 INTRODUCTION

High-precision measurements of the Cosmic Microwave Background (CMB) radiation by the *WMAP* satellite provide strong support for the so-called standard model of cosmic structure formation, in which Cold Dark Matter (CDM) and dark energy dominate the Universe. The matter distribution at the decoupling epoch has been directly probed by measurements of CMB anisotropies, and it has been confirmed that the observed matter distribution is consistent with the predictions of popular inflationary theories (Spergel et al. 2003). Within this theoretical framework, structure formation in the early Universe is described by gravitational amplification of small initial density fluctuations; non-linear evolution leads to the formation of dark matter halos, followed by hydrodynamic processes such as gas infall into gravitational potential wells, shock heating, and radiative cooling (e.g. Yoshida et al. 2003). Precise modelling of the angular power spectrum of the CMB anisotropies determines the relative densities of the baryonic and non-baryonic

components. Furthermore, accurate solutions of the non-linear Boltzmann equations (Hu & Sugiyama 1995; Ma & Bertschinger 1995; Seljak & Zaldarriaga 1996) show that there is a substantial difference in the distribution of baryons and dark matter at the decoupling epoch. Indeed, recent detailed numerical studies (Yamamoto, Sugiyama & Sato 1998; Singh & Ma 2002) show that the differences remain until much lower redshift $z \sim 20$ for high baryon densities. In fact, the ratio of baryon density to CDM density determined by the *WMAP* data (Spergel et al. 2003) is as large as $\Omega_{\text{baryon}}/\Omega_{\text{cdm}} \sim 0.2$. Thus these results clearly contradict the assumption, often made in the context of structure formation, that baryons trace the dark matter; i.e. that local baryon densities are just proportional to those of the dark matter, and their velocities are identical both in direction and in amplitude.

Numerical simulation of structure formation is aimed at revealing how the large-scale features of the Universe formed and evolved from high to low redshifts. Conventionally, cosmological N -body simulations are started from an initial matter distribution – a random Gaussian realisation – generated using an input power spectrum for the *total* matter

* E-mail: nyoshida@cfa.harvard.edu (NY)

density. Although this is obviously the most plausible way of generating initial conditions for N -body simulations with only a single collisionless component, it is non-trivial to realise the matter distribution in simulations that employ two (or more) components so that the density and velocity fields of both components evolve consistently. A common belief is that details in the initial configuration are erased by non-linear evolution and hence do not matter if one is interested in the structure of non-linear objects (i.e. “dark halos”) at low redshift. However, this reasoning may not apply at high redshifts or for the intergalactic medium (IGM) where the density fluctuations on relevant scales are in the linear to mildly non-linear regime.

In numerical studies of the properties of the IGM, such as those concerned with the reionisation history of the Universe (e.g. Gnedin & Ostriker 1997; Gnedin 2000; Sokasian et al. 2002, 2003), it is important to accurately compute the thermal properties of baryons in low density regions. Various analytic methods have been developed to obtain the local densities and temperatures of the IGM from the distribution of dark matter that can be computed relatively accurately by either direct N -body simulations or linear theory (e.g. Bi, Börner & Chu 1992; Jones 1996; Hui & Gnedin 1997; Nusser 2000; Matarrese & Mohayaee 2002). On the other hand, in cosmological N -body/hydrodynamic simulations, simplifying assumptions are often made. For example, in cosmological Smoothed Particle Hydrodynamics (SPH) simulations, gas particles are either put on top of dark matter particles, or simply displaced by half the mean interparticle separation before perturbations are imposed (e.g. Katz et al. 1996). A naive way of improving upon this simple approach would be to apply the Zel’dovich approximation to baryonic and dark matter components separately using separate transfer functions for each. It is unclear, however, if the generated initial particle distributions and the velocity field reproduce consistent results with predictions of full non-linear theory.

Another closely related issue is that, in particle simulations, a smooth density field must be represented by discrete mass elements. It is well-known that discretisation itself imposes some limitations on the accuracy of numerical simulations (Splinter et al. 1998; Hamana, Yoshida & Suto 2001; Baertschiger et al. 2002). Baertschiger & Sylos-Labini (2001) show that the discreteness of the particles contributes to the evolution of power-law clustering on small scales. Götz & Sommer-Larsen (2002) argue that even small differences in unperturbed particle distributions can yield quite different, in some cases unfavourable, results in the nonlinear evolution of systems (see their Fig. 1).

These facts and questions motivate the need for a systematic study in order to develop and verify a proper method for setting up initial conditions for multi-component cosmological simulations. In the present paper, we examine how details in the initial set-up affect the evolution of matter density fluctuations. We specifically study the power spectra of baryonic and dark matter components and the abundance of dark matter halos using a set of N -body simulations. We show that differences in initial configurations indeed result in substantial differences in the evolved density field and its growth rate. We compare the numerical results with theoretical predictions and determine an improved method for generating initial conditions.

The rest of the paper is organised as follows. In Section

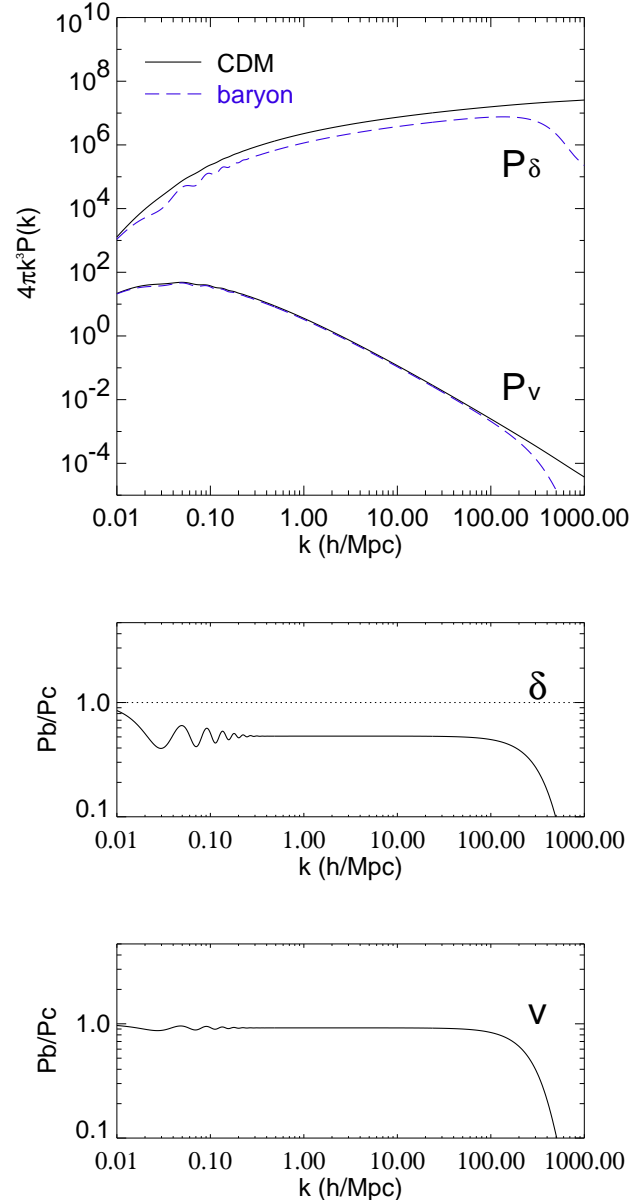


Figure 1. The density and velocity power spectra for CDM (solid line) and for baryons (dashed line) at $z = 100$ for a standard Λ CDM model with $\Omega_{\text{cdm}} = 0.26$, $\Omega_{\text{baryon}} = 0.04$, $\Omega_{\Lambda} = 0.7$, $H_0 = 70 \text{ km s}^{-1} \text{Mpc}^{-1}$. In the top panel, the relative amplitudes of the density to velocity power spectra are scaled arbitrarily. The middle panel shows the ratio of the two density power spectra and the bottom panel shows that of the two velocity power spectra.

2, we present the basic theory of the evolution of density fluctuations in the early Universe. In Section 3, we describe the simulation set. We show our numerical results in section 4. Discussion is given in Section 5.

2 THEORY

2.1 Evolution of baryon density fluctuations

The evolution of the cosmological baryon perturbations before the decoupling epoch is described by a number of physical processes which couple the perturbation fields of baryons, CDM, photons and neutrinos in a complex manner. One thus needs to solve the full set of coupled nonlinear Einstein-Boltzmann equations in order to obtain an accurate result. Recent detailed studies by Liu et al. (2001) and Singh & Ma (2002) show that, although density fluctuations on scales smaller than the photon diffusion scale (Silk 1968) are strongly suppressed, the growth of the baryon density fluctuations are eventually accelerated *during* the drag epoch because the photon-baryon coupling breaks down by recombination. It is also important to note that second-order effects arising from the coupling of the velocity fields to the baryon density field can enhance the growth of small scale fluctuations (Shaviv 1998; Liu et al. 2001; Singh & Ma 2002), although this effect plays an important role only on very small length scales ($k \gg 1000 \text{Mpc}^{-1}$).

After recombination, gravitational infall causes the baryon density fluctuations to catch up with those of the dark matter. Yamamoto et al. (1998) show, however, that the growth of perturbation modes on length scales smaller than the Jeans length is delayed due to the initial oscillatory behaviour of the baryons, and thus the residual differences in the fluctuation amplitudes between baryons and dark matter remain until redshifts $z \sim 20 - 100$. This is clearly shown in Figure 1. There we plot the density power spectra and the velocity power spectra for baryons and CDM for a conventional Λ CDM universe (parameters as summarised in Section 3) at $z = 100$. The power spectra are computed using the Boltzmann solver of Sugiyama (1995), as described in Yamamoto, Sugiyama & Sato (1998). The density power spectra for baryons and CDM differ by about a factor of two for $1 < k < 10$, whereas the difference in the velocity power spectra is less than 10 percent on these scales (compare the middle panel with the bottom panel).

2.2 The Zel'dovich approximation

The standard procedure for setting up initial conditions for cosmological N -body simulations is to perturb a uniform particle distribution using the Zel'dovich approximation (Zel'dovich 1970). An extensive study of the applicability of the Zel'dovich approximation is presented in a series of papers by Valageas (2002a,b and references therein). We summarise the elements of the method in this section.

Let the initial Lagrangian coordinate of a particle in an unperturbed distribution be \mathbf{q} . Then each particle is subject to a displacement corresponding to a density perturbation. In the Zel'dovich approximation the Eulerian coordinate of the particle at time t is

$$\mathbf{r}(t, \mathbf{q}) = a(t)[\mathbf{q} - b(t)\nabla_{\mathbf{q}}\Phi_0(\mathbf{q})], \quad (1)$$

where $\mathbf{r} = a(t)\mathbf{x}$ with \mathbf{x} being a comoving coordinate and $b(t)$ is the growth factor. The velocity field is obtained from

$$\mathbf{v} = a \frac{d\mathbf{x}}{dt} = -ab\dot{b}\nabla_{\mathbf{q}}\Phi_0(\mathbf{q}). \quad (2)$$

Table 1. Simulation sets

–	glass files	trans. func.	phase	velocity correction
Run A	same	diff	same	no
Run B	diff	diff	same	no
Run C	diff	diff	same	yes
Run D	same	same [†]	same	no
Run E	diff	diff	diff	no

† Transfer function for the total matter

The quantity $\Phi_0(\mathbf{q})$ is related to the density perturbation δ in the linear regime via the Poisson equation:

$$\delta = b\nabla_{\mathbf{q}}^2\Phi_0. \quad (3)$$

It is important to point out that the initial velocity field and the displacement field are linearly related via equation (2). Namely, particles in the Zel'dovich approximation execute motion on straight line trajectories. Therefore, if one uses different transfer functions for two components (e.g. CDM and baryons) while keeping the phase information for a random Gaussian field identical, the generated displacement fields and hence the velocity fields for the two components should differ by an amount corresponding to the difference in the amplitudes of the transfer functions. However, after the decoupling epoch, baryons fall into gravitational potential wells that are dominated by the dark matter, whereas the growth of dark matter density fluctuations is slightly delayed due to the baryonic matter which is more homogeneously distributed. Then, the difference in velocities of baryons and dark matter decays quickly after the decoupling epoch (compare the middle panel and the bottom panel in Figure 1).

Nusser (2000) and Matarrese & Mohayaee (2002) recently derived analytic solutions for the evolution of linear density perturbations for both baryons and dark matter. While their solutions fully describe the evolution of linear density fluctuations of a two-component fluid for a few particular cases, they are not directly applicable to generating initial conditions for direct N -body simulations in more general cases. In the present paper we develop a more practical method. The key question is *how can we generate initial conditions using solutions of a full non-linear calculation?*

We test five different methods for setting up initial conditions in order to distinguish a correct method (if one exists) and to quantify its accuracy. We describe the technical details in the next section.

3 THE N -BODY/SPH SIMULATIONS

We use the parallel N -body/SPH code GADGET (Springel, Yoshida & White 2001), in its “conservative entropy” version (Springel & Hernquist 2002, 2003). All our simulations employ 2×128^3 particles (CDM and non-radiative gas components) in a cosmological box of $4 h^{-1} \text{Mpc}$ on a side. We work with a flat Λ -dominated Cold Dark Matter universe, with matter density $\Omega_{\text{cdm}} = 0.26$, $\Omega_{\text{b}} = 0.04$, cosmological constant $\Omega_{\Lambda} = 0.7$ and expansion rate at the present epoch

$H_0 = 70 \text{ km s}^{-1} \text{ Mpc}^{-1}$. The qualitative features of our results are not affected by the adopted cosmology, although the degree of the numerical artifacts we discuss depend on the ratio of $\Omega_{\text{cdm}}/\Omega_{\text{b}}$. Table 1 summarises the five methods we consider for the set-up of the initial conditions. We describe each specifically in the following subsections. We note that for all the simulations we set the parameters governing the accuracy of the force calculation and time stepping to be very conservative, following Springel et al. (2001) and Power et al. (2003). We set the gravitational softening length $\epsilon_{\text{soft}} = 3 h^{-1} \text{ kpc} \sim$ one tenth of the mean inter-particle separation.

3.1 Unperturbed particle distribution

There are two popular methods for distributing particles “uniformly”. One is to place particles on a rectangular grid. While used most often, a grid distribution has the unfavourable feature of imposing a particular direction in the particle distribution. In other words, a grid distribution is not isotropic, although it is homogeneous on scales larger than the mean inter-particle separation (see e.g. Baertschiger & Sylos-Labini 2001). Götz & Sommer-Larsen (2002) report that grid distributions cause peculiar problems when used for warm dark matter simulations such as those of Bode, Ostriker & Turok (2001). Although the degree of these problems is somewhat uncertain and is likely to be case dependent, it is preferable to avoid these issues altogether by using “glass” particle distributions. Following White (1994), we generate glass initial conditions by evolving a gravitationally interacting N -particle system in an expanding background with the sign of gravity reversed such that each particle feels repulsive forces from all the other particles. When the system reaches a quasi-equilibrium state, unphysical clumping in the initial distribution is substantially damped, while maintaining uniformity. The particle distribution is also nearly isotropic and hence does not possess any preferred direction.

For all the numerical experiments in the present paper, we use glass particle distributions. We generate two independent glass distributions and use them for gas and CDM particles in Runs B, C, and E, whereas we use identical glass particle distributions for both components in Run A and D (see Table 1).

3.2 Transfer functions

In the context of structure formation in CDM models, the density power spectrum at a given epoch is related to the transfer function by

$$P(k) = Ak^n T^2(k), \quad (4)$$

where A is the normalization factor. We consider the Harrison-Zel’dovich primordial power spectrum with $n = 1$. Figure 1 shows the power spectrum $4\pi k^3 P(k)$ at $z_{\text{init}} = 100$. On very large length scales ($k < 0.01 h/\text{Mpc}$), the power spectra for baryons and CDM have the same amplitudes, whereas on intermediate length scales ($1 < k < 100$) the amplitudes for baryon density perturbations are smaller by about a factor of two at $z = 100$. Also the power spectrum for baryons shows characteristic wiggles at $0.01 < k < 0.2$

which is induced by Jeans oscillations before the recombination epoch.

For Runs A, B, and C, transfer functions are given separately for the CDM and the baryonic components, whereas for Run D, we use a single transfer function computed for the total matter density fluctuations. The matter transfer function for Run D is computed from

$$T(k) = \frac{\Omega_{\text{b}}}{\Omega_{\text{total}}} T_{\text{b}}(k) + \frac{\Omega_{\text{cdm}}}{\Omega_{\text{total}}} T_{\text{cdm}}(k). \quad (5)$$

3.3 Phases

In standard inflationary theories that predict adiabatic-type density fluctuations, the distribution of various forms of matter is described by essentially a single scalar function, and thus the phases for baryons and CDM are identical for all the perturbation modes. Although we have no compelling reason to assume the phases are different on any length scale, it is interesting to examine the effect of varying the phases. In order to make comparisons, we assign random, independent phase information for baryons and CDM in Run E. Other configurations for Run E are identical to those of Run B. We compare these simulations in Section 5.

3.4 Velocity power spectrum

As we have discussed in Section 2, the differences in the velocity power spectra of baryons and CDM are smaller than the differences in fractional amplitudes of density fluctuations (Figure 1). Since the fractional difference is within 10% and nearly a constant at $z_{\text{init}} = 100$ over most of the relevant scales, we approximate the velocity fields of both CDM and baryons by the velocity field of the *total* matter. In practice, we compute the velocity field using the transfer function for the total matter while keeping the phase information identical to that used in generating the spatial displacements. Note that this is equivalent to multiplying the velocity term in equation (2) by a scalar factor. The scalar factor could, in principle, be made scale-dependent, as is done by Klypin et al. (1997) for Mixed Dark Matter simulations.

4 RESULTS

Figure 2 shows the power spectra of the initial mass distribution for the four simulations (Run A, B, C, D), and the subsequent evolution is shown in Figure 2 (for $z = 50$) and Figure 3 ($z = 20, 30$). The filled circles are measured power spectrum for CDM and the open diamonds are for baryons. Note that the particular random realization for these runs shows a dip at $k \sim 3h/\text{Mpc}$. This is simply due to randomization when assigning the fluctuation amplitudes for each perturbation mode, and irrelevant to the analysis in the present paper. Theoretical predictions are shown by the solid line (CDM) and by the dashed line (baryon) for each output redshift. The measured power spectra at $z = 100$ show a steep turn-over at large wavenumbers $k > 20$ due to the Poisson noise which scales with the particle number N as $\langle |\delta_k|^2 \rangle = 1/N$. (Note that we plot $4\pi k^3 P(k)$ in Figures 2 and 3.) Although the level of the Poisson noise could be reduced by using a larger number of particles, we refrain from carrying out such large, costly simulations. Since we focus

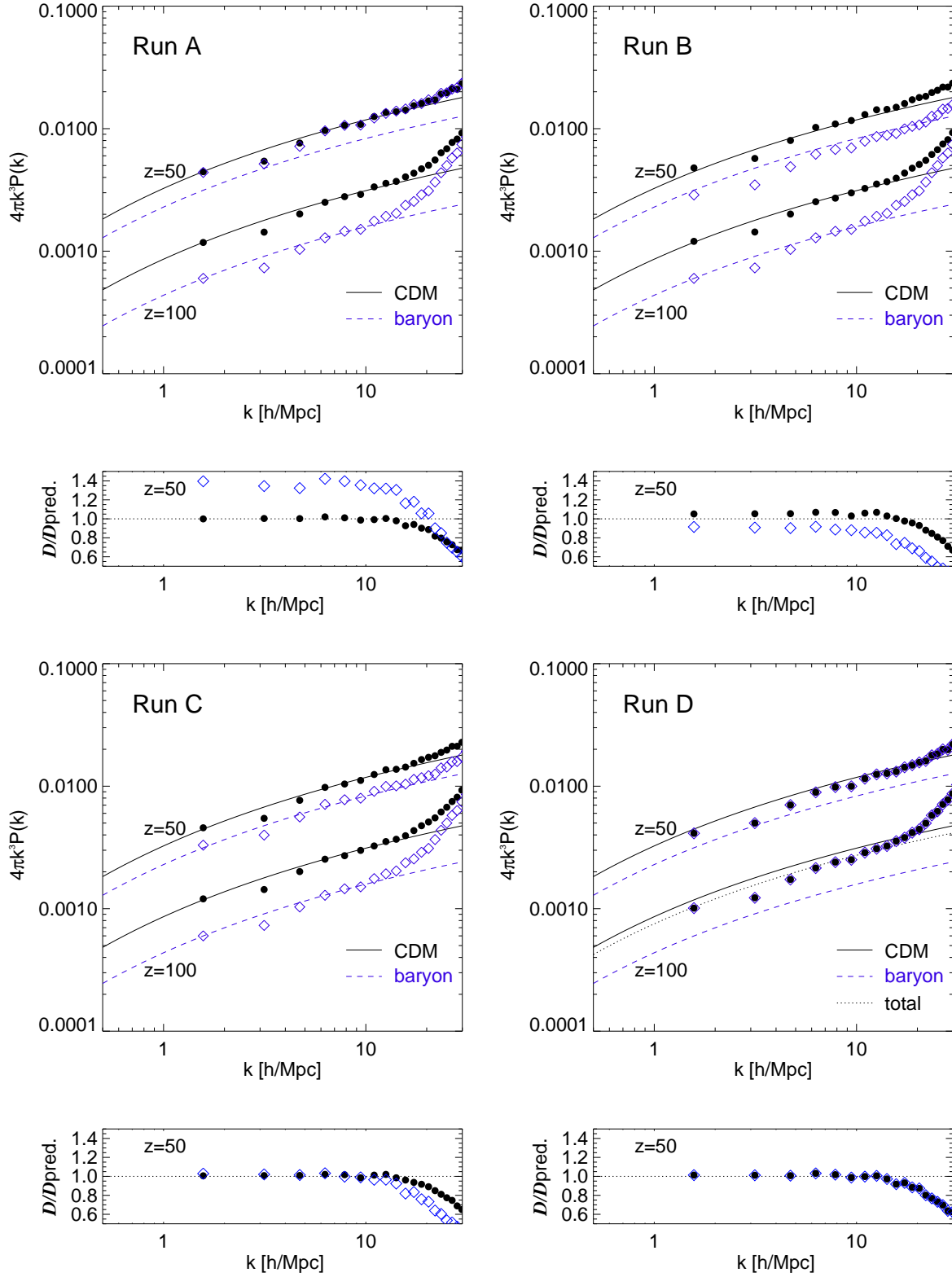


Figure 2. The measured power spectra for the baryonic and CDM components are compared with the theoretical predictions at the initial epoch ($z = 100$) and at $z = 50$. In each panel the top portion shows the power spectra $4\pi k^3 P(k)$ and the bottom portion shows the measured growth rate normalised by the theoretically expected value. Note the vertical axis in the bottom portion is in linear scale.

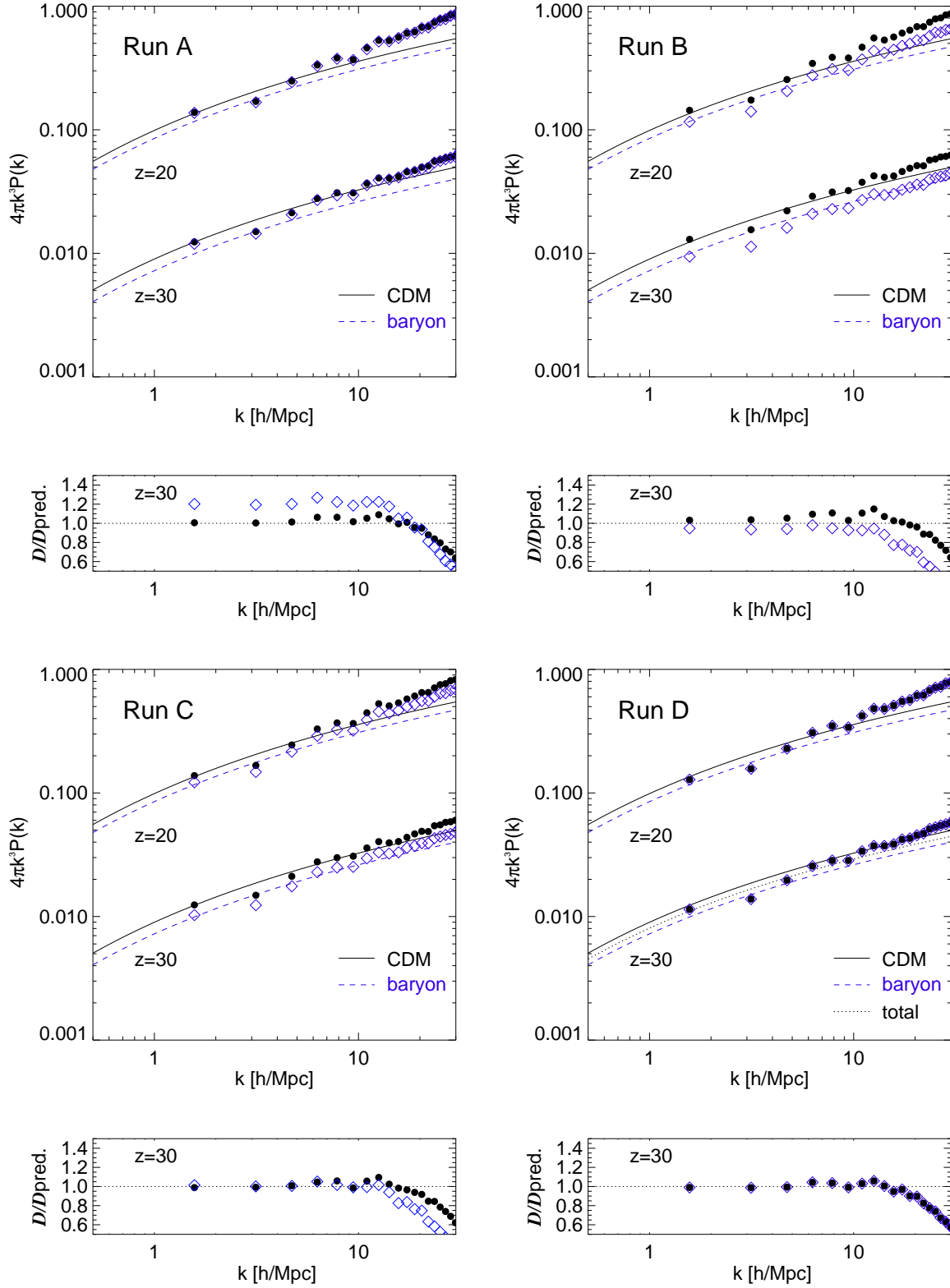


Figure 3. As for Figure 2, but for $z = 20$ and $z = 30$. The power spectra at $z = 20$ are scaled vertically by a constant factor of five, in order to clarify the plot

on density fluctuations on large length scales, $k < 20$, where the power spectra and the growth rates can be measured robustly, the shot noise effect is not important in the analysis presented in the following.

In Run D, baryons and CDM have exactly the same velocities both in amplitude and direction. For this simulation the gas particles are simply put on top of the CDM particles and thus they move together initially. Since we used the transfer function for the total matter density in Run D, the measured power spectrum for CDM is smaller than the theoretical prediction (solid line), whereas that for the baryons is larger than the theoretical prediction (dashed line). These differences can be easily accounted for by the ratio of Ω_{baryon} and Ω_{cdm} to Ω_{total} .

In the bottom portion of each panel in Figure 2, 3, we plot the growth rate of the densities. We measure the growth rate between $z_{\text{init}} (= 100)$ and z , normalised by theoretical prediction as

$$\frac{D}{D_{\text{pred}}} = \frac{P(k; z)/P(k; z_{\text{init}})}{P_{\text{pred}}(k; z)/P_{\text{pred}}(k; z_{\text{init}})}. \quad (6)$$

We compute the theoretical prediction directly from the result of the Boltzmann solver. Run C and Run D reproduce the theoretically predicted value very well, whereas other runs show substantial deviations from the prediction. This remains true even at $z = 30$, as shown in Figure 3.

The significant over-shoot of the baryonic component in Run A is explained by the tight coupling of the gas and CDM particles *falsely caused* by using correct transfer functions. In Figure 4, we plot the initial particle distributions in a slab of thickness $40 h^{-1} \text{kpc}$ for Run A (top panel) and Run B (bottom panel). Figure 4 clearly shows that the gas particles are placed too closely to the nearest CDM particles in Run A. Using separate transfer functions whose amplitudes differ by an approximately constant (and small) factor over the relevant length scales, one obtains a distribution of gas particles each of which is only slightly separated from the closest CDM particle. In this situation, a major fraction of the force exerted on a gas particle is due to the nearest CDM particle, which causes the gas particle to move faster than expected in linear theory. This false coupling was successfully avoided in RunB, for which we used two sets of independent glass distributions; one for the gas particles and the other for the CDM particles. Thus, the velocity vector of a gas particle is uncorrelated with the direction to the nearest CDM particle, as is seen in Figure 4.

Although Run B appears to behave reasonably well, CDM density fluctuations grow slightly too fast whereas the baryon density fluctuations grow too slowly, as seen in the growth rate in comparison with the theoretical prediction. The initial velocities are assigned separately to each component following the standard procedure of the Zel'dovich approximation. Without correcting velocities, the CDM density fluctuations grow faster than the correct solution, and the opposite is true for the baryons. This feature is not seen in Run C, because we corrected the initial velocities for both the baryonic and CDM components. Indeed, the density fluctuations in Run C grow almost precisely as predicted from $z_{\text{init}} = 100$ to $z = 20$.

Run D reproduces the correct growth of density fluctuations. This is as expected, because, in Run D, the two components initially behave as a single component, until

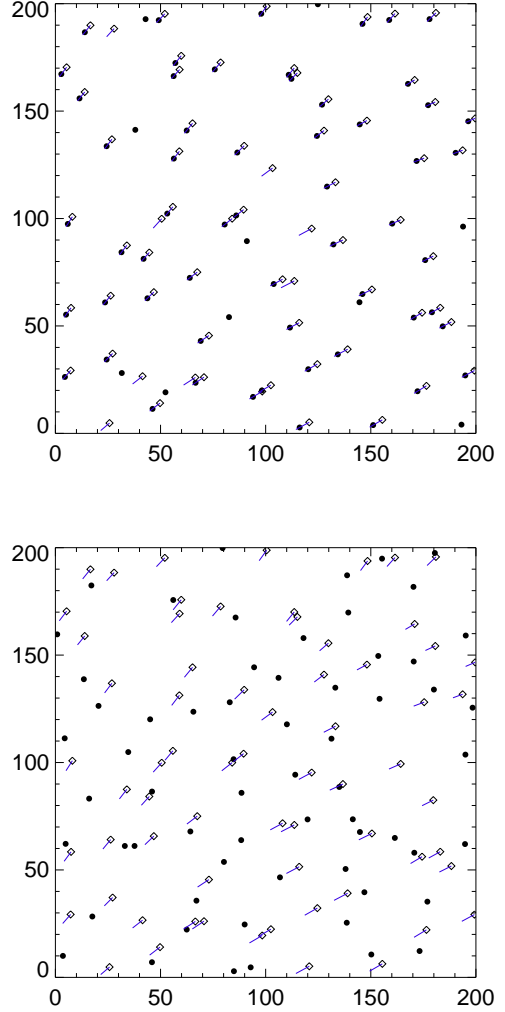


Figure 4. The initial particle distribution in a slab of thickness $40 h^{-1} \text{kpc}$ (1 percent of the box side-length) in Run A (top) and Run B (bottom). The solid points are CDM particles and the open diamonds are gas particles. The short lines originating from the gas particles show the velocity vectors.

the pressure forces on gas particles becomes important and, making the orbits of the gas and CDM particles deviate from each other. Note that, at any output redshift, the density fluctuations for a single component (baryons or CDM) does not accurately represent the true solution. Hence, we conclude that the set-up for Run D is not suitable for studies that are concerned with the difference in the distribution of baryons and dark matter.

Overall the initial set up for Run C is clearly the most favourable. The method used for Run C appears to eliminate all the problems and undesirable features found in the other simulations. Also, the excellent agreement between the measured power spectra and the theoretical prediction for *both* baryonic and CDM components over a large redshift interval confirms that the method is useful for the multi-component cosmological simulations.

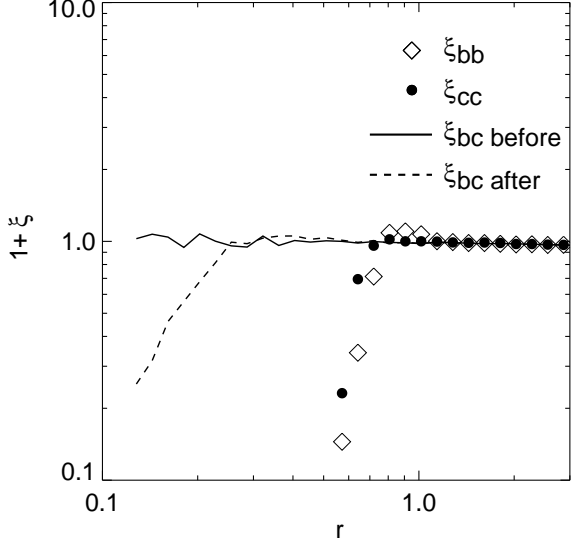


Figure 5. The two-point correlation function for the gas particles (ξ_{bb} , open diamonds) and for the dark matter particles (ξ_{cc} , solid circles) in a glass distribution. The solid line shows the cross-correlation ξ_{bc} computed for an arbitrary superposition of two independent glass files, whereas the dashed line is the cross-correlation measured for the distribution of the mixture of the two components after they were evolved for a brief period (see text). The separation length r is normalised by the mean inter-particle separation.

5 DISCUSSION

5.1 Glass distribution for two components

Although the comparison of the results of Run A and Run B show the advantage of using two glass distributions for the CDM and baryonic components, it remains unclear whether the mixture of two independent glass distributions still possesses all desired features. Generally it does not, because close encounters between particles from the different components could happen (Jun Makino, private communication). In order to address this issue, we compute the cross-correlation function ξ_{bc} for a mixed glass distribution. We make a distribution for 2×128^3 particles by arbitrarily superposing a glass distribution for 128^3 particles on another glass distribution which is independently generated. The solid line in Figure 5 shows the gas-dark matter cross-correlation ξ_{bc} for this arbitrary mixture of two sets of glass distributions. The overall behaviour might seem quite good, as the cross-correlation ξ_{bc} stays at an almost constant value around zero. However, it means that there is some chance that a gas particle finds a CDM particle quite close to it. Since this chance coupling of the two different components can cause exactly the same problem, even locally, as we found in Run A, it is preferable to generate a distribution of the two components such that the cross-correlation between them is reduced on very small scales. We follow the same procedure as we have done to create glass distributions; i.e., we switch the sign of the gravitational force and evolve the system consisting of a mixture of 2×128^3 particles in an expanding background. Since our primary purpose is to avoid false coupling of gas and dark matter particles, we evolve

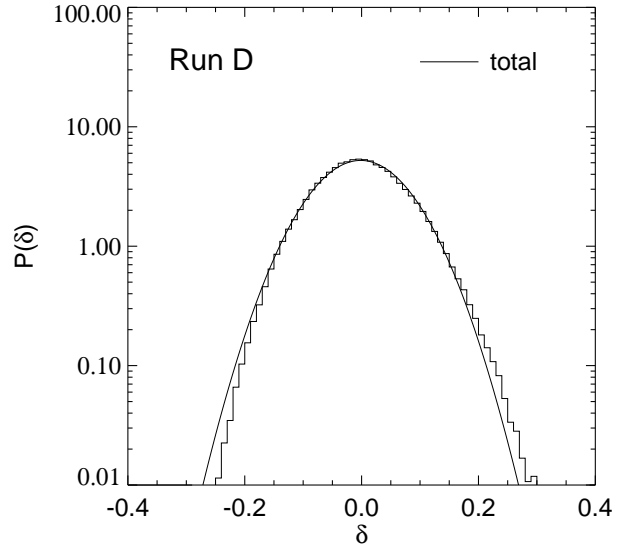
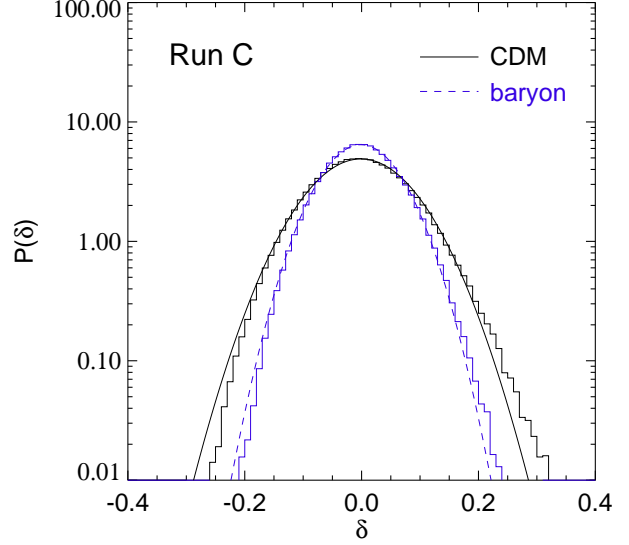


Figure 6. The probability distribution $P(\delta)$ for the initial conditions for Run C (top) and Run D (bottom). In Run D, the CDM and gas particles have identical distributions and hence $P(\delta)$ is also identical initially.

the system only for a brief period of time. Figure 5 shows the cross-correlation function for the initial (solid line) and evolved (dashed line) mixture of the particles. We also plot the correlation of the gas particles (open diamonds) and that of the CDM particles (solid circles). Figure 5 shows that the glass distribution we obtained in this manner possesses the following desired properties: (1) the correlation of a single component is reduced on scales below the mean-interparticle separation, and (2) the cross-correlation is also reduced on the small scales, confirming that the false coupling with the other component such as that found in Run A will not be induced even when we use separate transfer functions.

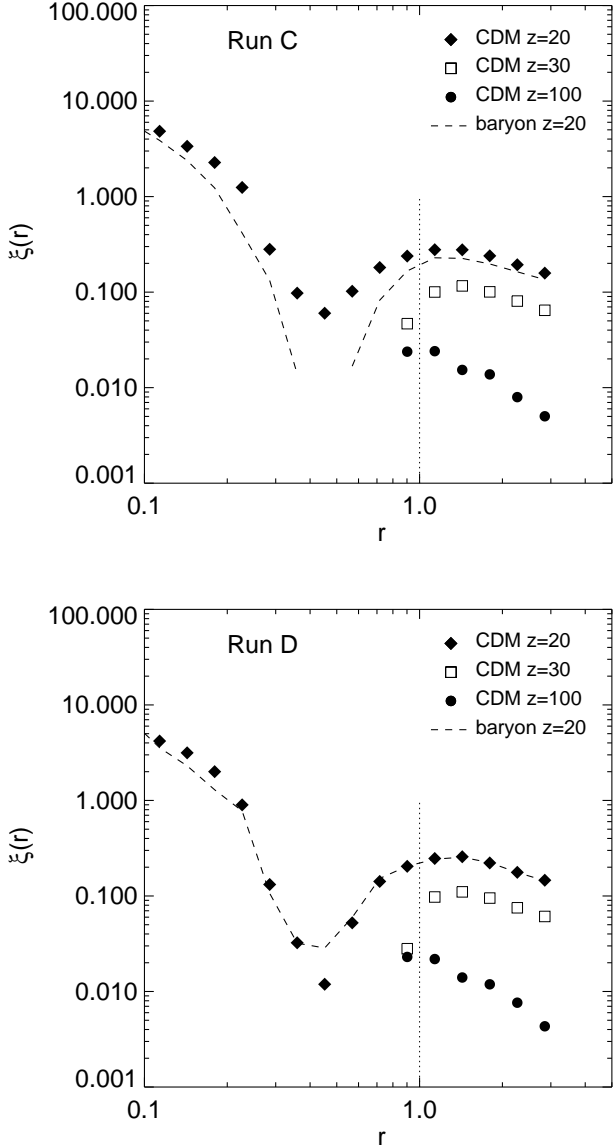


Figure 7. The evolution of the two-point correlation function for Run C (top) and Run D (bottom). Symbols are for the dark matter component, as indicated in the legend in each panel, and the dashed line is the correlation function of the baryonic particles at $z = 20$. The separation length r is normalized by the mean inter-particle separation.

5.2 Real space correlation on small scales

While we conclude that glass distributions are preferred over a regular grid distribution for the reasons described in the previous sections, there still remain a few issues to be clarified regarding unperturbed particle distributions. Setting-up initial conditions for cosmological particle simulations is generally divided into two parts. One is the generation of a uniform particle distribution, which we have discussed, and the other is imposing desired density fluctuations by displacing the particles using the Zeldovich approximation (section 2.2). For the currently standard cosmological models, we further assume that the initial density field is a Gaussian

random field, for which the power spectrum fully describes the statistical properties. We first check and show that the initial particle distribution generated in this manner represents a Gaussian density field. i.e., the probability distribution $P(\delta)$ of overdensity $\delta(x) = \rho/\bar{\rho} - 1$ in real space is Gaussian. Figure 6 shows $P(\delta)$ for our Run C and Run D. We compute the real space density $\delta(x)$ by first re-sampling the particles onto a 128^3 grid and then smoothing on a scale $R_s = 100h^{-1}\text{kpc}$. For Run C, we compute $P(\delta)$ for both the baryonic and dark matter components, whereas for Run D only the dark matter component is used. (Note that in Run D the gas particles are put on top of the dark matter particles initially, and hence $P(\delta)$ at the initial epoch is identical.) As clearly seen in Figure 6, the computed probability distribution is well fitted by a Gaussian for each case. The difference between the two components in Run C is due to the difference in the linear power amplitude on the chosen length scale $R_s \sim 100h^{-1}\text{kpc}$. The measured variances for the baryonic and dark matter components are $\sigma_b=0.062$, $\sigma_{\text{cdm}}=0.081$, respectively, in good agreement with analytical estimates $\sigma_{\text{th},b}=0.060$, $\sigma_{\text{th},\text{cdm}}=0.083$ computed from the input density power spectra. The corresponding numbers for Run D are $\sigma_{\text{total}}=0.076$ and $\sigma_{\text{th},\text{total}}=0.078$. We note that, in practice, we used a random number generator in assigning the phases for each Fourier mode so that the generated initial conditions possess a desired feature of a Gaussian random field.

Since any particle distribution (e.g. glass or grid) has its own intrinsic correlations (Gabrielli et al. 2002), the perturbed distribution will have, in principle, a superposition of the intrinsic and imposed (desired) correlations. Baertschiger & Sylos-Labini (2002) argue that the desired power law correlations for cosmological models are not properly realized in discretised density fields at the initial epoch (see also Knebe & Dominguez 2003). We quantify and show this feature by computing the real space correlation from particle distributions. We use the pair-count estimator proposed by Landy & Szalay (1993):

$$\xi(r) = \frac{DD(r) - 2DR(r) + RR(r)}{RR(r)}. \quad (7)$$

We randomly distribute the same number of particles as the actual simulation particle, and evaluate the data-data (DD), data-random (DR), and random-random (RR) terms to obtain $\xi(r)$. In Figure 7 we show the two-point correlation functions measured from the outputs of Run C and Run D. Initially the correlation on scales below the mean inter-particle separation (dotted line) is absent, reflecting the damped correlation on the small scales in the unperturbed distribution (see Figure 5). The particle clustering at early epochs on the smallest scales is considerably affected by the discreteness as argued by Hamana, Yoshida & Suto (2002). Baertschiger et al. (2002) claim that the development of a power-law correlation on the small scales is governed partly by the initial clustering. It is interesting that the two-point correlation functions of the two components at $z = 20$ are quite similar even on the smallest length scales, despite the fact that they started from *different* glass distributions. On the other hand, the feature that the correlation amplitudes are different between the two components in Run C is plausible, and it appears to reproduce correctly the smaller density fluctuations of baryons. At late epochs the nonlinear power trans-

fer eventually dominates the initial power if the effective spectral index at the scale $n \equiv d \log P(k) / d \log k$ is much less than -1 . CDM models satisfy this condition on small length scales (Suto & Sasaki 1991), and hence the power on scales below the mean particle separation at later epochs is expected to be generated via nonlinear mode-coupling (Sugimoto et al. 1991; Hamana et al. 2002). Further theoretical study is clearly needed to understand the behaviour of the small scale correlations at early epochs.

5.3 Differing phases

As we discussed in Section 3.3, the phases of the perturbations are assumed to be identical for baryons and dark matter as long as the density perturbations are in the linear regime. Nevertheless, it is interesting to examine how the growth of density fluctuations is affected by offsets of phases between the two components. We note that, in real astrophysical situations, phase offsets may be caused during early reionization when the intergalactic gas is photo-heated by radiation from an early generation of stars and driven out of dark matter potential wells. In such cases, it is expected that the growth of either or both components is delayed, compared to the case where the phases are synchronised. We carry out a simple test by applying independent phases to baryon and CDM perturbations at the initial epoch. For simplicity, we assign completely random phases, rather than specifying actual mechanisms that could cause such an offset. Hence, the test is meant to show the effects of the phase offset qualitatively. Figure 8 shows the evolution of the density fluctuations for Run E. As expected, the evolution of both the baryon and the CDM density fluctuations is delayed, with the effect on the former being more substantial. On the other hand, it is interesting that the growth of the baryon density fluctuations is not entirely prevented, despite the large difference in the fractional densities between the two components. This is because, on large scales, the dark matter density fluctuations are still small and the gravitational force from the dark matter has not significantly changed the initial momentum of the baryonic components. Note that, in Figure 8, the apparent differences between the measured power spectra and the theoretical prediction should be interpreted to be owing mostly to the difference in the background assumption, because the theoretical prediction itself is obtained assuming the initial phases are identical.

5.4 Nonlinear objects

In the previous sections, we have focused on the evolution of density fluctuations on large scales when they are in linear regime. As Figure 2 and Figure 3 show, the overall differences between our simulations appear as if their effective growth factors deviate, falsely or due to an inaccurate set-up, from the *true* value. This raises an interesting question of whether or not such differences also show up in some properties of non-linear objects. Using our simulations, we identify dark matter halos by running a friend of friends (FOF) group-finder with the standard choice of linking parameter $b = 0.164$. We first consider only the dark matter component. The baryon fraction within the halos will be examined later in this section. Figure 9 shows the cumulative

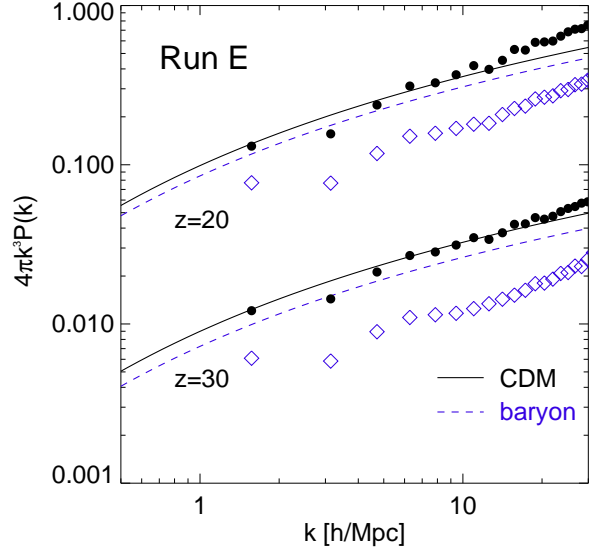


Figure 8. The evolution of the power spectra in Run E. As in Figure 3, the power spectra at $z = 20$ are scaled vertically by a constant factor of five, in order to clarify the plot.

mass functions for our simulations at $z = 20$ and $z = 15$. Since the overall abundance of halos is still small at $z = 20$, as seen in the top panel in Figure 9, we allow our simulations to evolve to $z = 15$ to have a large number of halos. We show the result for the $z = 15$ outputs in the bottom panel of Figure 9. We compute the mass of the identified halos to be the number of member particles times the particle mass. We discard halos consisting of fewer than 25 particles, and thus the minimum mass in our sample is set to be $5 \times 10^7 h^{-1} M_{\odot}$. Although the mass functions measured in the four simulations agree reasonably well, there is an appreciable differences, particularly between Run D and the other runs. This is easily accounted for by the fact that the growth of the dark matter density fluctuations in Run D is slower than the other runs (see Figure 2, 3).

We also measured the baryon fraction within the dark halos. To this end, we compute the virial radii and virial masses for the halos following Yoshida et al. (2002). Briefly, we define the virial radius R_{vir} as the radius of the sphere centred on the most bound particle of the FOF group having overdensity 200 with respect to the critical density. The virial mass M_{vir} is then the enclosed mass (gas and dark matter) within R_{vir} . We compute the baryon fractions for the halos as $f_b = M_{\text{gas}} / M_{\text{total}}$, and normalise by the global baryon fraction $\Omega_b / \Omega_{\text{matter}}$. Figure 10 shows the measured baryon fractions for the halos in our simulation at $z = 15$. In all cases the (normalised) baryon fractions are smaller than unity, representing correctly the effect of hydrodynamic pressure in the absence of gas cooling. Whereas the large scatter at masses smaller than $\sim 2 \times 10^8 h^{-1} M_{\odot}$, consisting of fewer than 100 particles, is due to the mass resolution (see Yoshida et al. 2002 for a discussion of the resolution issue), the difference on larger mass scale between the four runs is unexpected. Again, by noting the residual difference in the baryon and dark matter density fluctuations shown in Figure 3 and Figure 7, we are led to the conclusion that

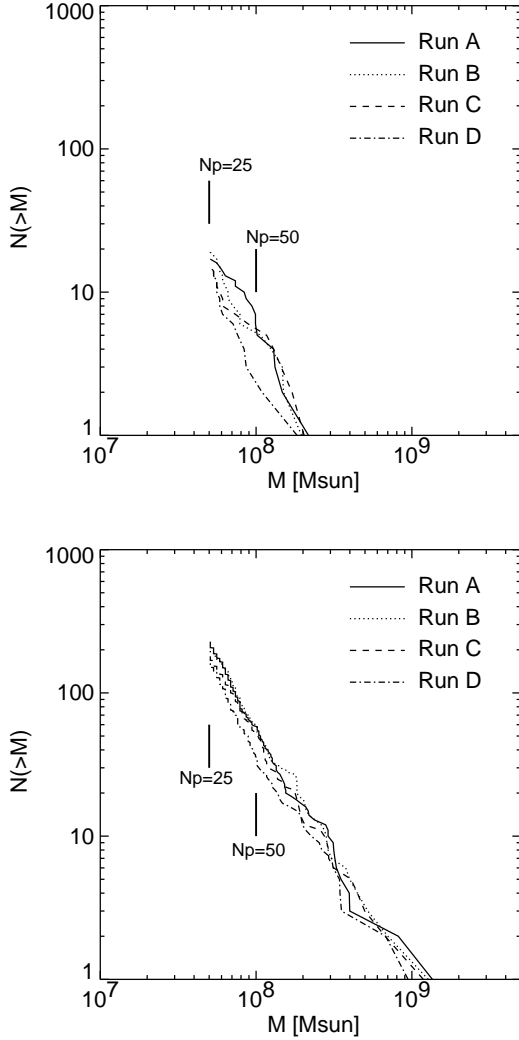


Figure 9. Cumulative mass function of dark matter halos at $z = 20$ (top) and $z = 15$ (bottom). The vertical lines indicate the number of particles constituting a halo of a corresponding mass.

the difference in the density fluctuations at early epochs is responsible for the overall trend shown in Figure 10. Indeed, the amplitudes of the baryon and dark matter density fluctuations in Run A and Run D are quite similar from early on ($z \sim 50$), while those in Run B and Run C remain relatively large until low redshift ($z \sim 20$). Thus the gas infall is slightly delayed in Run B and Run C, resulting in the smaller baryon fractions than in Run A and Run D.

It should be noted that these results are not expected to be precise in details, but are likely to be dependent on the procedure for identifying halos and also on the definition of the halo mass. The detailed description of nonlinear evolution is beyond the scope of our paper and thus we reserve this issue for the subject of future work using simulations with substantially higher resolution than those described here.

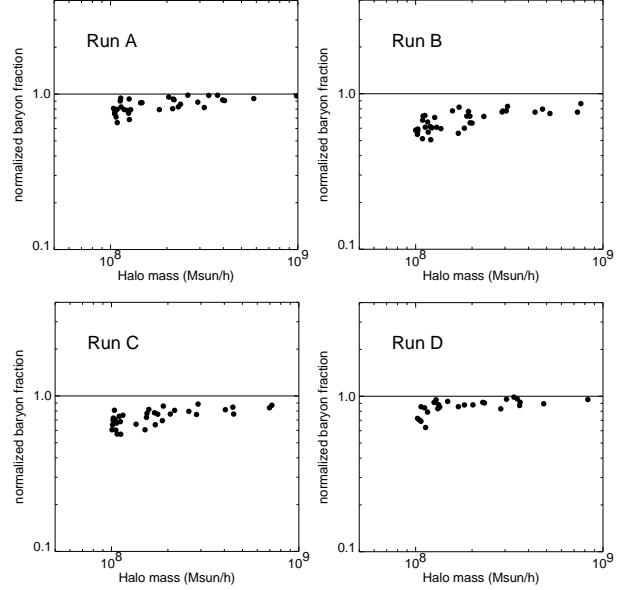


Figure 10. Baryon fractions for massive ($M > 10^8 h^{-1} M_\odot$) halos at $z = 15$. The baryon fractions are normalised by the global baryon fraction $\Omega_{\text{baryon}}/\Omega_{\text{matter}}$.

6 CONCLUSION

We have studied the evolution of the matter density fluctuations in cosmological N -body/hydrodynamic simulations, and discussed various aspects of the set-up of the initial conditions. All the methods we used in generating the initial conditions except for Run E may appear to be *plausible*, differing only in a few details. However, we have found that such seemingly minor details cause appreciable differences in the evolved density field, not only in linear regime but also in the non-linear regime.

Interestingly, it has turned out that neither of the methods used for Run A and Run D provide suitable initial conditions, with the results of the former being more significantly affected by numerical artifacts. This perhaps comes as a surprise, particularly in the case of Run A, because one may naively hope that using separate transfer functions for baryons and CDM would produce more accurate results. In fact, the baryon density fluctuations reproduced in Run A are the least accurate in terms of the growth rate. Although the particular problem of false particle coupling found in Run A is likely to be a problem in simulations where both components are represented by discrete mass elements, it is preferable, even in simulations that employ a grid-based Eulerian scheme, to avoid artificial coherence between the initial fluid velocity vector and the direction to the nearest CDM particle. This may deserve further study using a grid-based scheme.

By analysing the outputs of the numerical experiments, we identified some peculiar problems and inaccuracies caused by the simplest methods. Then, based on the results, we have suggested a more accurate method to set up initial conditions; i.e., the one used for Run C. In summary, we recommend: (1) using independent glass particle distributions from which a “glass mixture” is made by a treatment to avoid false coupling, (2) using two transfer functions com-

puted for baryons and for dark matter, *and* (3) taking into account the difference in their velocities at the initialisation epoch. We emphasize that the latter two procedures may be necessary for all cosmological simulations employing multiple components, whether or not both dark matter and gas are realised with particles. We have explicitly shown that, in this manner, the evolution of matter density fluctuations are accurately followed at high redshift.

ACKNOWLEDGMENTS

We thank Edmund Bertschinger, Chung-Pei Ma, Matias Zaldarriaga, Hugues Mathis and Takashi Hamana for valuable discussion. We also thank the anonymous referee for giving constructive comments which improved the manuscript. This work was supported in part by NSF grants ACI 96-19019, AST 98-02568, AST 99-00877, and AST 00-71019, and by NASA ATP grant NAG5-12150. The simulations were performed at the Center for Parallel Astrophysical Computing at the Harvard-Smithsonian Center for Astrophysics.

REFERENCES

- Baertschiger, T. & Sylos-Labini, F., 2001, *Europhys. Lett.*, 568, 455
 Baertschiger, T., Joyce, M. & Sylos-Labini, F. 2002, *ApJL*, 581, 63
 Bi, H. G., Börner, G. & Chu, Y., 1992, *A&A*, 266, 1
 Bode, P., Ostriker, J. P. & Turok, N., 2001, *ApJ*, 556, 93
 Gabrielli, A., Joyce, M. & Sylos Labini, F., 2002, *Phys. Rev. D*, 65, 083523
 Gnedin, N. Y. & Ostriker, J. P., 1997, *ApJ*, 486, 581
 Gnedin, N. Y. 2000, *ApJ*, 535, 530
 Götz, M. & Sommer-Larsen, J., 2002, preprint astro-ph/0210599
 Hamana, T., Yoshida, N. & Suto, Y., 2001, *ApJ*, 568, 455
 Hu, W. & Sugiyama, N., 1995, *ApJ*, 444, 489
 Hui, L. & Gnedin, N. Y., 1997, *MNRAS*, 292, 72
 Jones, B. J. T., 1999, *MNRAS*, 307, 376
 Katz, N., Weinberg, D.H. & Hernquist, L. 1996. *ApJS*, 105, 19
 Klypin, A., Nolthenius, R. & Primack, J., 1997, *ApJ*, 474, 533
 Knebe, A. & Dominguez, A., 2003, *PASA* 20, 1
 Landy, S. D. & Szalay, A. S. 1993, *ApJ*, 412, 64
 Liu, G.-C., Yamamoto, K., Sugiyama, N & Nishioka, H. 2001, *ApJ*, 547, 1
 Ma, C.-P., & Bertschinger, E. 1995, *ApJ*, 455, 7
 Matarrese, S. & Mohayaee, R. 2002, *MNRAS*, 329, 37
 Nusser, A., 2000, *MNRAS*, 317, 902
 Power, C. et al. 2003, *MNRAS*, 338, 14
 Seljak, U. & Zaldarriaga, M. 1996, *ApJ*, 469, 437
 Shaviv, N. J. 1998, *MNRAS*, 297, 1245
 Silk, J. 1968, *ApJ*, 151, 459
 Singh, S. & Ma, C.-P. 2002, *ApJ*, 569, 1
 Sokasian, A., Abel, T., Hernquist, L. & Springel, V. 2003, *ApJ*, submitted [astro-ph/0303098]
 Sokasian, A., Abel, T., & Hernquist, L. 2002, *MNRAS*, 332, 601
 Spergel, D.N. et al. 2003, *ApJ*, submitted [astro-ph/0302209]
 Splinter, R. J., Melott, A. L., Shandarin, S. F. & Suto, Y. 1998, *ApJ*, 497, 38
 Springel, V. & Hernquist, L. 2002, *MNRAS*, 339, 312
 Springel, V. & Hernquist, L. 2003, *MNRAS*, 333, 649
 Springel, V., Yoshida, N., & White, S. D. M., 2001, *New Astronomy*, 6, 79
 Sugiyama, N., Suto, Y., Bouchet, F. & Hernquist, L., 1991, *ApJS*, 75, 631
 Sugiyama, N., 1995, *ApJ*, 100, 281
 Suto, Y. & Sasaki, M., 1991, *Phys. Rev. Lett.*, 66, 264
 Valageas, P. 2002a, *A&A*, 385, 761
 Valageas, P. 2002b, *A&A*, 382, 412
 White, S. D. M., 1994, in Schaeffer, R., Silk, J., Zinn-Justin, J., eds. *Cosmology and Large Scale Structure*, Les Houches Lectures
 Yamamoto, K., Sugiyama, N. & Sato, H., 2001, *ApJ*, 501, 442
 Yoshida, N., Stoehr, F., Springel, V. & White, S. D. M. 2002, *MNRAS*, 335, 762
 Yoshida, N., Abel, T., Hernquist, L. & Sugiyama, N., 2003, *ApJ*, in press [astro-ph/0301645]
 Zel'dovich, Ya. B., 1970, *A&A*, 5, 84